PCCP

PAPER

View Article Online
View Journal

Cite this: DOI: 10.1039/c9cp03638e

Multi-particle momentum correlations extracted using covariance methods on multiple-ionization of diiodomethane molecules by soft-X-ray free-electron laser pulses

Daehyun You,[a] Hironobu Fukuzawa,*[ab] Yu Luo,[a] Shu Saito,[a] Marta Berholts,[c] Thomas Gaumnitz,[d] Marko Huttula,[e] Per Johnsson,[f] Naoki Kishimoto,[g] Hanna Myllynen,[c] Ahmad Nemer,[ah] Akinobu Niozu,[bi] Minna Patanen,[e] Eetu Pelimanni,[e] Tsukasa Takanashi,[a] Shin-ichi Wada,[j] Naomichi Yokono,[i] Shigeki Owada,[b] Kensuke Tono,[k] Makina Yabashi,[b] Kiyonobu Nagaya,[bi] Edwin Kukk[ac] and Kiyoshi Ueda[ab]

Received 28th June 2019,
Accepted 15th August 2019

DOI: 10.1039/c9cp03638e

rsc.li/pccp

Momenta of ions from diiodomethane molecules after multiple ionization by soft-X-ray free-electron-laser pulses are measured. Correlations between the ion momenta are extracted by covariance methods formulated for the use in multiparticle momentum-resolved ion time-of-flight spectroscopy. Femtosecond dynamics of the dissociating multiply charged diiodomethane cations is discussed and interpreted by using simulations based on a classical Coulomb explosion model including charge evolution.

1 Introduction

Currently, seven short-wavelength free-electron-laser (FEL) facilities are in user operation world-wide.[1–7] These short-wavelength FELs have created new opportunities in many research fields, for example making possible the determination of structures of non-crystalline samples[8–10] and of matter in transient states.[11–15] The FEL radiation pulses used in such structural studies exhibit extreme peak intensities compressed into a duration as short as one femtosecond. Consequently, highly relevant in these studies is the femtosecond-scale behaviour of matter exposed to such extreme intensity of light.

Absorption of the intense FEL pulses may lead to both geometrical and electronic distortions of the original object, often ultimately causing the complete destruction of the object. A central issue of this context is the time-scale in which the original object's structure is sufficiently preserved. If the structure of the object is to be determined, the relevant information should be captured before the distortion occurs.[16–18] In this respect it is vital to study the interaction between the intense FEL pulses and various forms of matter, which is also a topic of fundamental interest in its own right.[19–30] In the absorption of a FEL radiation pulse in small quantum systems, the ensuing dynamics exhibits a complex interplay between the electronic and nuclear motions. In order to study in detail such coupled motion of electrons and ions, a single molecule composed of a small number of atoms is an ideal target, since various levels of theory and experimental methods are available.

Erk *et al.* investigated ionization and fragmentation of methylselenol (CH_3SeH) molecules by intense ($<10^{17}$ W cm^{-2}), 5 fs-long pulses of 2 keV energy at the LCLS FEL facility, using coincident ion momentum spectroscopy.[24] At SACLA, we investigated reaction dynamics of iodomethane (CH_3I), the simplest I-substituted hydrocarbon,[31] diiodomethane (CH_2I_2) that has two X-ray absorption sites,[32] and 5-iodouracil ($C_4H_3IN_2O_2$), abbreviated as 5-IU, more complex molecule of biological relevance,[33,34] irradiated by intense ($<10^{17}$ W cm^{-2}), 10 fs-long X-ray pulses of 5.5 keV energy, using coincident ion momentum spectroscopy. We also investigated, by the same technique, the molecular dynamics of tetrabromothiophene (C_4Br_4S) using approximately 70 fs-long soft-X-ray pulses of 130 eV energy.[35]

We carried out simulations based on a classical Coulomb explosion model including charge evolution (CCE-CE), which

[a] Institute of Multidisciplinary Research for Advanced Materials, Tohoku University, Sendai 980-8577, Japan. E-mail: fukuzawa@tohoku.ac.jp; Fax: +81-22-217-5380; Tel: +81-22-217-5383
[b] RIKEN SPring-8 Center, Sayo, Hyogo 679-5148, Japan
[c] Department of Physics and Astronomy, University of Turku, Turku FI-20014, Finland
[d] Laboratorium für Physikalische Chemie, ETH Zürich, Zürich, 8093, Switzerland
[e] Nano and Molecular Systems Research Unit, Faculty of Science, University of Oulu, P. O. Box 3000, 90014 Oulu, Finland
[f] Department of Physics, Lund University, Lund SE-22100, Sweden
[g] Department of Chemistry, Graduate School of Science, Tohoku University, Sendai 980-8578, Japan
[h] Department of Physics, Auburn University, AuburnAlabama 36849, USA
[i] Department of Physics, Kyoto University, Kyoto 606-8502, Japan
[j] Department of Physical Science, Hiroshima University, Higashi-Hiroshima 739-8526, Japan
[k] Japan Synchrotron Radiation Research Institute (JASRI), Sayo, Hyogo 679-5198, Japan

accounts, by including a few empirical time constants, for the concerted dynamics of charge build-up, charge redistribution and nuclear motion. The CCE-CE simulations were performed for CH_3I,[31] 5-IU,[33] and C_4Br_4S,[35] and a self-consistent charge density-functional-based tight-binding (SCC-DFTB) method for 5-IU,[34] CH_3I and CH_2I_2.[32] When both models – CCE-CE and SCC-DFTB – were applied (to 5-IU and CH_3I), they both reproduced well the observed ion momentum values and correlations. The two modelling approaches are also complementary – we found that the SCC-DFTB modelling, in which the influence of molecular bonds (that are neglected in CCE-CE) is taken into account, in some cases reproduces the experiments better than CCE-CE.[34] In the SCC-DFTB modelling, however, we could not include unbalanced charge build-up scenarios in the two iodine ions in the case of CH_2I_2.[32] Also, the SCC-DFTB modelling could not take into account the charge redistribution time.[32,34] Based on the experiments[31,33] interpreted with the help of the CCE-CE simulations, we concluded that the charge build-up in the absorption hot-spots takes about ten fs, while it is redistributed among atoms in only a few fs.

Here, we report an extension of our FEL-induced fragmentation studies of CH_2I_2 to the soft X-ray range, using SACLA BL1 and employing 70 fs pulses at the photon energy of 93 eV. We interpret the results with the help of CCE-CE model, so that the different final charges of the two iodine fragments can be taken into account. We aim at finding the influence from different properties of FEL pulses (photon energy and pulse duration) to the molecular fragmentation dynamics, by comparing the present soft X-ray results with the previous hard X-ray results and referring to the different time constants obtained from the CCE-CE simulations when reproducing both experiments.

Before presenting the results, an important issue in moving from hard to soft X-ray region is worth pointing out, namely that the total photoionization cross-section of the sample is significantly larger in the latter. The ionization cross-sections of residual gases such as H_2O and of He that is employed as a sample carrier gas are also more than a thousand to hundred thousand times larger. Thus, the number of sample molecules ionized in a pulse can be much higher than one, in addition to the many residual-gas and carrier-gas ions. Accurate and detailed event-by-event information on the aforementioned ion yield and momentum correlations can be obtained by coincidence analysis. In its basic form, it relies on a single target molecule being the source of all collected ions per pulse. When more than one molecule is ionized in a pulse, the chance of combining fragment ions from different molecules – creating false coincidences – occurs, with a probability rapidly increasing with the average ionization rate per pulse. As a result, if we were to employ the coincidence analysis as in the previous hard X-ray experiments,[24,31–33] the false-to-true coincidence ratio would be significantly larger. This is a rather common problem in soft X-ray FEL experiments of this kind.

There are several methods to partially overcome the false coincidence problem and to extract only true coincidences.[35–39] One method commonly used is the three-dimensional (3D) momentum filter method that is based on momentum conservation law (see, *e.g.* ref. 39, a review applying it to FEL experiments). It relies on a good momentum correlation between fragments. Thus, in fragmentation of larger molecules where the momenta of an ion pair are often only very weakly correlated, the method loses its efficiency. In combination with and in addition to the momentum filter, the false coincidence contributions to various statistics extracted from the coincident dataset can be estimated by deliberately combining ions from different pulses (scrambling), thus destroying all true coincidences. The momentum filter-scrambling combination was successfully used in the soft X-ray regime in the analysis of C_4Br_4S,[35] but it is still limited to relatively low ionization rates.

In the present work we investigate the application of a statistical method – covariance analysis[36,38] – instead of the event-by-event coincidence analysis technique. The mathematically elegant covariance analysis approach has the advantage of being usable at high ionization rates and for high false coincidence contributions, thus being especially suitable for FEL experiments in the soft X-ray regime.

Section 2 describes the experiment. Section 3 describes covariance methods we employed for the data analysis. Section 4 describes the experimental result analysed by two-fold and three-fold covariances and Section 5 is the discussion of the results in comparison with various scenarios in CCE-CE simulations.

2 Experiment

The experiments were carried out at the beamline BL1 of SACLA.[40] The photon energy was set to be 93 eV and bandwidth of it was $\sim$4 eV (FWHM). The duration of the FEL pulses was $\sim$70 fs (FWHM). The repetition rate of the FEL pulses were 60 Hz. Shot-by-shot pulse energies were measured by gas monitor detectors located upstream of the beamline. The pulse energy of the FEL pulse was $\sim$100 μJ in average at upstream of the beamline. The standard deviation of the FEL intensity distribution is 13% of the average. We attenuated FEL intensity by a zirconium filter of 1 μm thickness. The pulse energy at the focal point was estimated to be 4.6 μJ in average by measured pulse energy after the filter and throughput of the beamline. The FEL pulses were focused by a Kirkpatrick–Baez (KB) mirror system to a focal size of 5.3 μm × 5.1 μm (FWHM × FWHM). From those values the peak fluence of the FEL pulse was estimated to be 0.15 μJ μm^{-2}.

CH_2I_2 (99.7%) was purchased from Nacalai Tesque, Inc. and used without further purification. The gas phase sample was introduced to the focal point of the FEL pulses as a pulsed supersonic gas jet seeded in helium gas. The ions were detected by a multi-coincidence recoil-ion momentum spectrometer to measure 3D momenta for each fragment ion.[41] The molecular beam was crossed with the focused FEL beam at the focal point, and the emitted ions were projected by electric fields onto a microchannel plate (MCP) detector, in front of a three-layer-type delay-line anode (HEX120 from Roentdek GmbH).[42] We used velocity-map-imaging (VMI) electric field conditions.[43] Signals from the delay-line anode and MCPs were recorded by a digitizer and analysed by a software discriminator.[44] The arrival time and the arrival position of each ion were determined and allowed us to extract the 3D momentum of each ion. With the

voltage settings of the spectrometer, we could extract all singly charged ions ejected in all directions with kinetic energy up to $\sim$50 eV $\times$ Q, where Q is the charge number of ions.

3 Covariance analysis

In this section, we provide a general overview of covariance methods applied to the data analysis of coincident ion momentum spectroscopy. We first explain two-fold covariance and then extend it to three-fold covariance.

3.1 Two-fold covariance

The covariance Cov[X,Y] between two random variables X and Y is defined as:

$$\mathrm{Cov}[X,Y] \equiv E[(X - E[X])(Y - E[Y])] = E[XY] - E[X]E[Y] \tag{1}$$

where $E[X]$ is the average of X. We measure these as functions of independent variables u and v in spaces U and V, respectively. u and v can be any physical quantities that can also have different dimensions. Let us assume we measure the distributions f_i and g_i with respect to each event i, that is a FEL pulse in the present case. f_i and g_i are the functions from spaces U and V to one-dimensional (1D) real space R, respectively. Then the covariance between

$$X = \left\{ \int_{U'} f_i(u)\mathrm{d}u \right\}_i \tag{2}$$

and

$$Y = \left\{ \int_{V'} g_i(v)\mathrm{d}v \right\}_i \tag{3}$$

with subsets $U' \subset U$ and $V' \subset V$ of interest can be expressed as:

$$\begin{aligned} \mathrm{Cov}[X,Y] &= \int_{U'\times V'} \mathrm{d}u\mathrm{d}v E\left[\{f_i(u)g_i(v)\}_i\right] \\ &\quad - E\left[\{f_i(u)\}_i\right]E\left[\{g_i(v)\}_i\right] \\ &= \int_{U'\times V'} \mathrm{d}u\mathrm{d}v \mathrm{Cov}\left[\{f_i(u)\}_i, \{g_i(v)\}_i\right]. \end{aligned} \tag{4}$$

Thus, we regard a covariance Cov[X,Y] as the integrated value of a covariance function from $U \times V$ to R in a corresponding region $U' \times V'$. We will generalise this idea and apply it to any subsets $C' \in C \equiv U \times V$ including subsets which cannot be expressed by a product $U' \times V'$. of any subsets $U' \subset U$ and $V' \subset V$

$$\int_{C'} \mathrm{d}u\mathrm{d}v \mathrm{Cov}\left[\{f_i(u)\}_i, \{g_i(v)\}_i\right]. \tag{5}$$

The actual data we record in coincident, momentum-resolving ion time-of-flight (TOF) spectroscopy can be expressed as a series of flight times and ion hit coordinates on the detector. The events i are the FEL pulses, each of which can produce multiple ions. We can formally express such data using the sum of delta-functions δ with multidimensional spaces U and V as:

$$\begin{aligned} f_i(u) &= \sum_{n_i} \delta(u - u_{i,n_i}), \quad u_{i,n_i} \in U, \\ g_i(v) &= \sum_{m_i} \delta(v - v_{i,m_i}). \quad v_{i,m_i} \in V, \end{aligned} \tag{6}$$

Here serials $\{u_{i,n_i}\}_{n_i}$ and $\{v_{i,m_i}\}_{m_i}$ describe multiply detected particles for each event i, with each particle labelled by n_i or m_i. These functions allow us to analyse the covariance by using the combinations of counts of particles in a corresponding region $C' \subset C$

$$\begin{aligned} &\int_{C'} \mathrm{d}u\mathrm{d}v \mathrm{Cov}\left[\{f_i(u)\}_i, \{g_i(u)\}_i\right] \\ &= \frac{1}{N}\sum_i \int_{C'} \mathrm{d}u\mathrm{d}v \sum_{n_i,m_i} \delta(u - u_{i,n_i})\delta(v - v_{i,m_i}) \\ &\quad - \frac{1}{N^2}\sum_{i,j} \int_{C'} \mathrm{d}u\mathrm{d}v \sum_{n_i,m_j} \delta(u - u_{i,n_i})\delta(v - v_{j,m_j}), \end{aligned} \tag{7}$$

where N is the number of events. The first term of eqn (7) counts the combinations (u_{i,n_i}, v_{i,m_i}) within each event i of detected particles which meet a certain condition C'. This term is the same as coincidence counts without false coincidence background subtraction. The second term takes all combinations (u_{i,n_i}, v_{j,m_j}) of detected particles without limiting a combination to a single event i and counts them that satisfy the condition. One can interpret the second term as false correlations, an equivalent to the false coincidence background removal.

When the region C' can be written as a product $U' \times V'$ with $U' \in U$ and $V' \in V$, we can simplify eqn (7) to:

$$\begin{aligned} &\int_{U'\times V'} \mathrm{d}u\mathrm{d}v \mathrm{Cov}\left[\{f_i(u)\}_i, \{g_i(v)\}_i\right] \\ &= \frac{1}{N}\sum_i \int_{U'\times V'} \mathrm{d}u\mathrm{d}v \sum_{n_i,m_i} \delta(u - u_{i,n_i})\delta(v - v_{i,m_i}) \\ &\quad - \frac{1}{N}\sum_i \int_{U'} \mathrm{d}u \sum_{n_i} \delta(u - u_{i,n_i}) \frac{1}{N}\sum_j \int_{V'} \mathrm{d}v \sum_{m_j} \delta(v - v_{j,m_j}). \end{aligned} \tag{8}$$

Since the second term of eqn (8) does not require taking combinations, it can be computed with fewer computer resources. The time required to calculate the second term of eqn (8) is proportional to N. On the other hand, the time to calculate the second term of eqn (7) is proportional to N^2. Thus, by using eqn (8), one can expect shortening of the time required. When we cannot use eqn (8), *i.e.*, when C' cannot be written by $U' \times V'$, we sampled events to compute the second term of eqn (7). For example, when we measure correlation between two ion-TOFs, U and V will be 1D spaces of each ion TOF and u and v are variables that belong to the TOF-spaces U and V. Then, the region C' corresponding to the covariance between certain TOF regions can be written by TOF-region $\times$ TOF-region, *i.e.*, $U' \times V'$. In this case we can use eqn (8). However, when we consider momentum sum correlated with two ions, U and V will be 3D momentum spaces of each ion and

C' will be a certain region of the 3D momentum sum. The region of momentum sum cannot be expressed as a product of the momentum regions of the two ions. In this case, we cannot use eqn (8).

3.2 Three-fold covariance

Let us extend two-fold covariance to multidimensional covariances. First, multidimensional covariance Cov[X,Y,Z,...] of random variables X, Y, Z,... is defined as:

$$\mathrm{Cov}[X,Y,Z,\ldots] \equiv E[(X - E[X])(Y - E[Y])(Z - E[Z])\ldots]. \tag{9}$$

We can extend the present method to higher dimensions using eqn (9).

Here, we focus on three-fold covariance. We could rewrite eqn (9) as:

$$\begin{aligned}\mathrm{Cov}[X,Y,Z] = {} & E[XYZ] - E[X]E[YZ] - E[Y]E[ZX] \\ & - E[Z]E[XY] + 2E[X]E[Y]E[Z]\end{aligned} \tag{10}$$

The spectra of each event i can be expressed with discrete functions f_i, g_i and h_i from specific spaces U, V and W to real space R, respectively:

$$\begin{aligned} f_i(u) &= \sum_{n_i} \delta(u - u_{i,n_i}), \quad u_{i,n_i} \in U, \\ g_i(v) &= \sum_{m_i} \delta(v - v_{i,m_i}), \quad v_{i,m_i} \in V, \\ h_i(w) &= \sum_{l_i} \delta(w - w_{i,l_i}), \quad w_{i,l_i} \in W, \end{aligned} \tag{11}$$

where $u \in U$, $v \in V$ and $w \in W$ are variables. Here serials $\{u_{i,n_i}(u)\}_{n_i}$, $\{v_{i,m_i}(v)\}_{m_i}$ and $\{w_{i,l_i}(w)\}_{l_i}$ describe detected particles for each event i, with each particle labelled by n_i, m_i or l_i. By substituting the serials of the functions $\{f_i\}_i$, $\{g_i\}_i$ and $\{h_i\}_i$ into random variables X, Y and Z in eqn (10), and integrating them in a corresponding region $C' \in C \equiv U \times V \times W$, we obtain three-fold covariance:

$$\begin{aligned} &\int_{C'} \mathrm{d}u\mathrm{d}v\mathrm{d}w \mathrm{Cov}\left[\{f_i(u)\}_i, \{g_i(v)\}_i, \{h_i(w)\}_i\right] \\ &= \frac{1}{N}\sum_i \int_{C'} \mathrm{d}u\mathrm{d}v\mathrm{d}w \sum_{n_i,m_i,l_i} \delta(u - u_{i,n_i})\delta(v - v_{i,m_i})\delta(w - w_{i,l_i}) \\ &- \frac{1}{N^2}\sum_{i,j} \int_{C'} \mathrm{d}u\mathrm{d}v\mathrm{d}w \sum_{n_i,m_j,l_j} \delta(u - u_{i,n_i})\delta(v - v_{j,m_j})\delta(w - w_{j,l_j}) \\ &- \frac{1}{N^2}\sum_{i,j} \int_{C'} \mathrm{d}u\mathrm{d}v\mathrm{d}w \sum_{n_j,m_i,l_j} \delta(u - u_{j,n_j})\delta(v - v_{i,m_i})\delta(w - w_{j,l_j}) \\ &- \frac{1}{N^2}\sum_{i,j} \int_{C'} \mathrm{d}u\mathrm{d}v\mathrm{d}w \sum_{n_j,m_j,l_i} \delta(u - u_{j,n_j})\delta(v - v_{j,m_j})\delta(w - w_{i,l_i}) \\ &+ \frac{2}{N^3}\sum_{i,j,k} \int_{C'} \mathrm{d}u\mathrm{d}v\mathrm{d}w \sum_{n_i,m_j,l_k} \delta(u - u_{i,n_i})\delta(v - v_{j,m_j})\delta(w - w_{k,l_k}). \end{aligned} \tag{12}$$

Eqn (12) is consist of two parts as in the case of eqn (7): the first term and the other terms. The first term is the same as coincidence counts including both true and false correlations. The other terms represent the false correlations.

3.3 Application to the experimental data

In this subsection we apply three-fold covariance analysis to extract momentum correlations of three ions C^+, I^{2+} and I^+, originating from the Coulomb explosion of multiply charged CH_2I_2 molecules. In this example, u_{i,n_i}, v_{i,m_i} and w_{i,l_i} would correspond to the three components of the C^+, I^{2+} and I^+ momentum vectors, respectively. We identify the ions by their TOFs. The region C' is intersections of a corresponding bin region of interest, *e.g.* momentum sum or kinetic energy sum as we will show later in Fig. 1 and 2, respectively, and additional filters such as a 3D momentum filter.[39] Hereafter, we refer to covariance values multiplied by the number of shots as "counts".

Fig. 1(a) shows distributions of the y-component of momentum sum for C^+–I^{2+}–I^+ ions. The y axis is orthogonal to both the photon propagation direction and the ion flight direction in the spectrometer. Distributions labelled "Total" and "Random" show components expressed by the first term and the sum of other terms, respectively, of eqn (12). The "Total" and "Random" distributions correspond to those of "total coincidence" and "false coincidence" signals in the conventional coincidence analysis. Distributions labelled "True" are results from the covariance analysis. They correspond to the "true coincidence" distributions. The contributions from false correlations are subtracted by the covariance method. Here, we did not employ a 3D momentum filter, only selected the individual ions by their TOFs.

Fig. 1(b) depicts distributions when momentum sum of three ions is restricted to be $\leq$200 a.u. Momentum magnitude distributions of C^+, I^{2+}, and I^+ are peaked at $\sim$150, $\sim$300 and $\sim$300 a.u., respectively, in the true correlations. However, there is still a chance of the momenta of falsely combined ions accidentally nearly cancelling each other, so the contributions from random correlations are not zero and the momentum

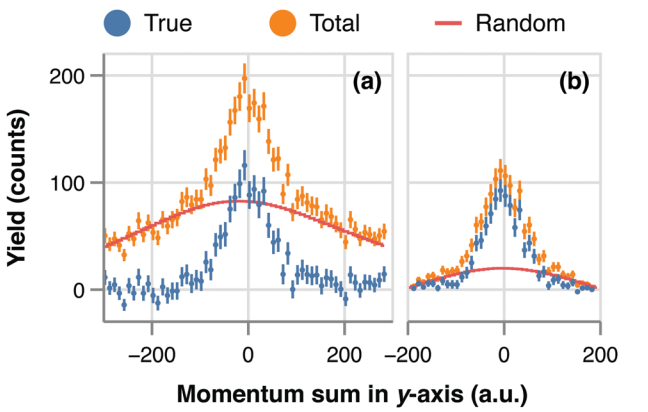

Fig. 1 Distributions of the y component of momentum sum for C^+–I^{2+}–I^+ ions. (a) Three ions are selected only by TOFs. (b) Momentum sum of three ions are restricted to be $\leq$200 a.u.

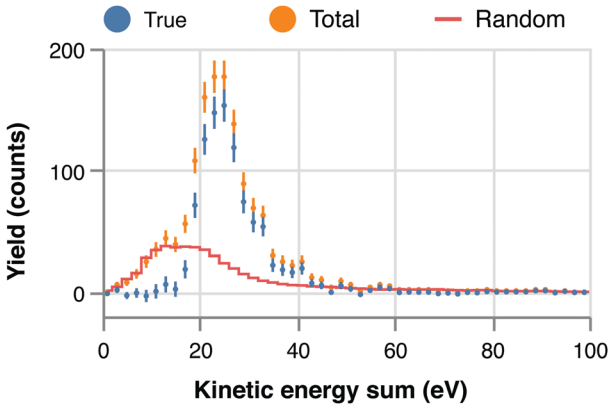

Fig. 2 Distributions of the kinetic energy sum for C^+–I^{2+}–I^+ ions. The momentum sum is restricted to be ≤200 a.u. as the same as Fig. 1(b).

sum distribution obtained by the covariance method gives a smaller peak. It indicates that a certain amount of ion combinations released from different molecules remain in the momentum filter method, but can be eliminated by the covariance method. It is noticeable that when we apply the covariance method with the 3D momentum filter, the distribution is basically the same as the distribution obtained by the covariance method without filtering but statistical errors become smaller. Thus we use the covariance method with the 3D momentum filter in the following.

As an example of the effectiveness of the covariance method, the kinetic energy sum distributions of the C^+–I^{2+}–I^+ ions are shown in Fig. 2. Distributions by only the momentum filter are also shown for comparison as labelled "Total". At low energy, there are contributions which cannot be removed by the momentum filter method. It is because when kinetic energies of randomly detected three ions are low, momentum sum is low. Thus such three ions slip through the momentum filter. Such random correlations could be removed also using a similar way, the scrambling method, which create false coincidences by picking up ion-detection information from different events.[35] An advantage to use the covariance method proposed is that it is free from normalization factors to subtract random correlations from total correlations. Note that ratio of intensities of the random correlations to true correlations increases when number of ions in one FEL shot increases. Thus when ion count rates are small as previous measurements,[31–33] contributions from the random correlations after the momentum filter are negligible.

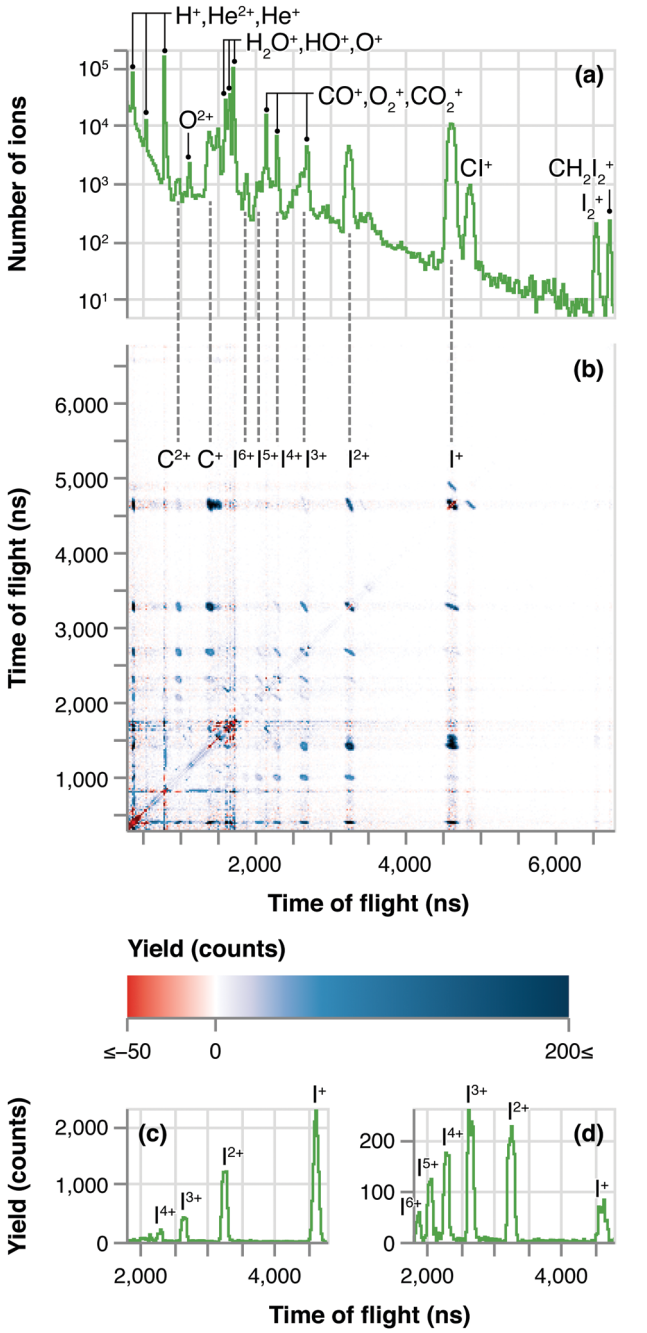

Fig. 3 Ion TOF spectra of CH_2I_2 recorded at FEL photon energy of 93 eV, plotted on a log scale. (a) Non-coincident ion spectrum. Dashed lines indicate expected TOFs for C^{l+} (l = 1, 2) and I^{m+} (m = 1–6) with zero kinetic energy. (b) Ion-TOF-ion-TOF covariance map. Counts are indicated by colour as shown in a colour bar. (c) Ion-TOF correlated with C^+. (d) Ion-TOF correlated with C^{2+}.

4 Results

4.1 Two-fold covariance

Let us first review the fragmentation pattern of multiply charged CH_2I_2 employing two-fold covariance. Fig. 3(a) depicts the ion TOF spectrum of CH_2I_2. It is not clear from this spectrum whether charge states higher than I^{2+} are present, since ions with shorter TOF than ~3000 ns overlap with the contributions of possible residual gases and helium. We can however clearly see fragment ions from CH_2I_2 in ion-TOF-ion-TOF covariance map in Fig. 3(b). In this map, we can see correlations between two ions and confirm the carbon ions charged up to +2 and iodine ions charged up to +6. It is noticeable that we could see clear correlations in the two detected ions although we expect non-detected ions have significant momenta. In such a situation, true correlations are

difficult to be extracted by the momentum filter method. The ions charged higher than C^{2+} and I^{6+} could not be extracted successfully because of extremely strong contributions from He^+ and H_2O^+, respectively. Fig. 3(c) and (d) depict the ion TOFs correlated with C^+ and C^{2+}, respectively. It is clear that the average charge state of iodine ions increases when the charge state of carbon ion goes from +1 to +2.

4.2 Three-fold covariance

We now investigate correlations of three ions using three-fold covariance. Fig. 4(a) and (b) present counts of the C^+ and two iodine ions and C^{2+} and two iodine ions detections, respectively, ejected from the FEL-irradiated CH_2I_2. One can see that the highest pair counts occur with almost equal charge partitioning. Relatively symmetric charge distributions illustrate a rather efficient equalisation of charge. Such efficient charge redistribution in a molecule must mean strong electronic interaction, such as in the form of molecular orbital formation that are then involved in the latter stages of the Auger cascades. But it is also clear from the figure that the charge equalisation is not always complete – it can be interrupted by the concurrent dissociation process. The average combined charge values of two iodine ions correlated with C^+ and C^{2+} are 3.8 and 5.9, respectively. Those are significantly lower than the results using 5.5 keV FEL, 5.5 and 7.2 for C^+ and C^{2+}, respectively.[32]

From the triple-ions correlation data, we can also extract the kinetic energy distributions of individual ions, as well as the distributions of kinetic energy sum for these ions. As typical examples we present the results for the C^+–I^{2+}–I^+ and C^{2+}–I^{4+}–I^3 ions in Fig. 5(a) and (b), respectively. The centre and the width

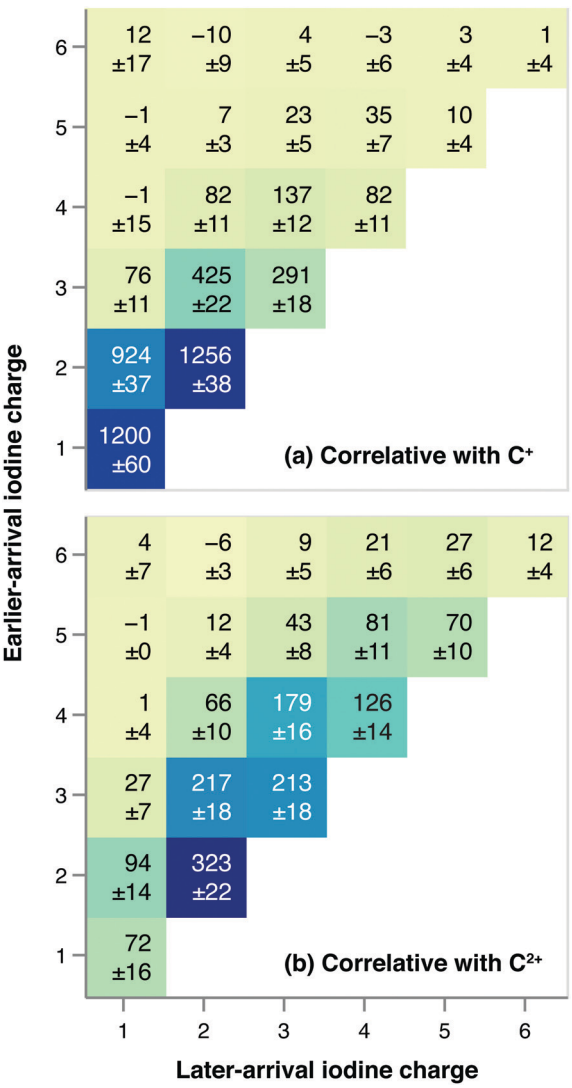

Fig. 4 Charge partitioning between the two iodine ions correlating with carbon charge states (a) C^+ and (b) C^{2+}. Intensity given as the total counts minus random correlation counts with errors given as standard deviation of statistical uncertainties.

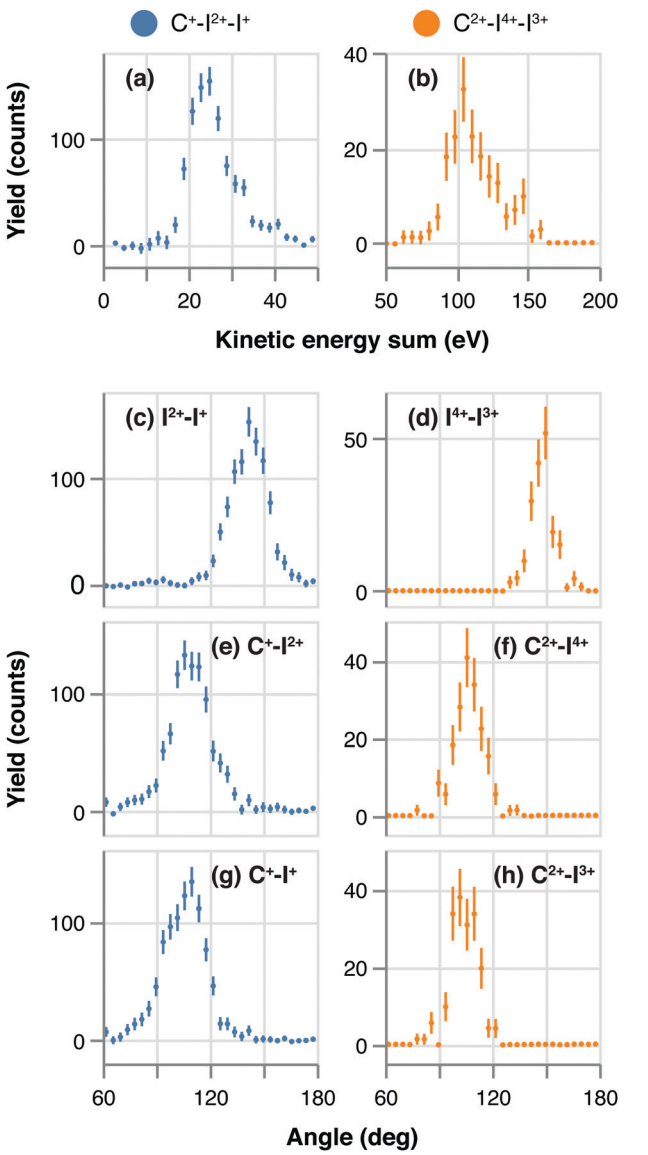

Fig. 5 Distributions of kinetic energy sum of (a) C^+–I^{2+}–I^+ ions and (b) C^{2+}–I^{4+}–I^{3+}. Angular distributions between two momenta of (c) I^{2+} and I^+ ions, (e) C^+ and I^{2+} ions and (g) C^+ and I^+ ions in the C^+–I^{2+}–I^+ production and (d) I^{4+} and I^{3+} ions, (f) C^{2+} and I^{4+} ions and (h) C^{2+} and I^{3+} ions in the C^{2+}–I^{4+}–I^{3+} production.

of the distribution increases with the increase in final charge, while the shape of the distribution remains nearly the same irrespective of the final charge. Angular distributions between the momenta of two of three ions, *i.e.*, two iodine ions, carbon and first iodine ions, carbon and second iodine ions, are also shown in Fig. 5. One can see that there are no significant changes for the centre of the angular distributions between different charge states.

For an overall view of charge state dependence, the averages of kinetic energy sum for various ion combinations and average angles between momenta of two of three ions are summarised in Fig. 6 and 7, respectively. For comparison, results from 10 fs long 5.5 keV FEL[32] are also shown. Kinetic energy sums in the present experiment are slightly lower (~94% in average) than those in the 5.5 keV, whereas there are no significant differences in average angles between the present and 5.5 keV results. The average angles between momenta of two iodine ions are larger than the angle of 118 degrees between two C–I bonds in the ground state CH_2I_2 molecule. They also increase when the charges of the two iodines increase. It is due to Coulomb repulsion between the two iodines.

5 Discussion

In order to obtain dynamical information, we have carried out a series of simulations based on a classical Coulomb explosion model including charge evolution (CCE-CE) where only

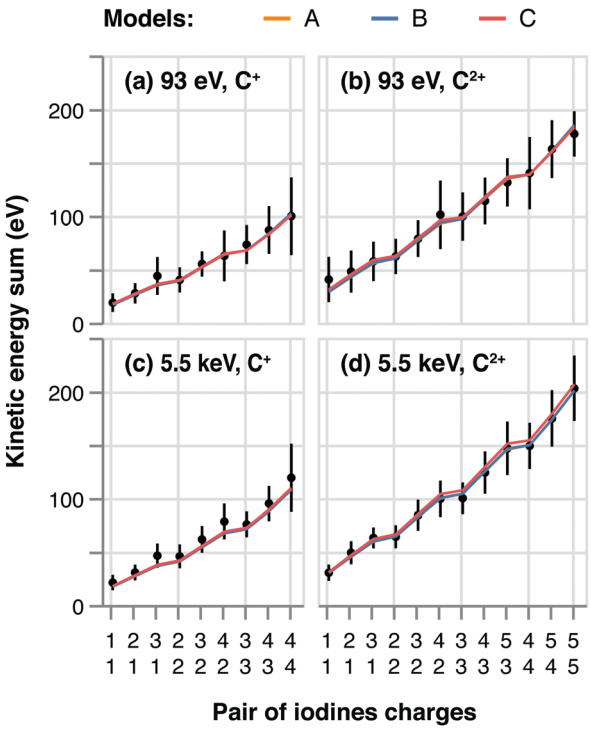

Fig. 6 Averages of kinetic energy sum for three ions include (a) C^+ and (b) C^{2+} at 93 eV FEL photon energy and (c) C^+ and (d) C^{2+} at 5.5 keV. The data in (c) and (d) used to generate the experimental plots are the same as those reported in ref. 32.

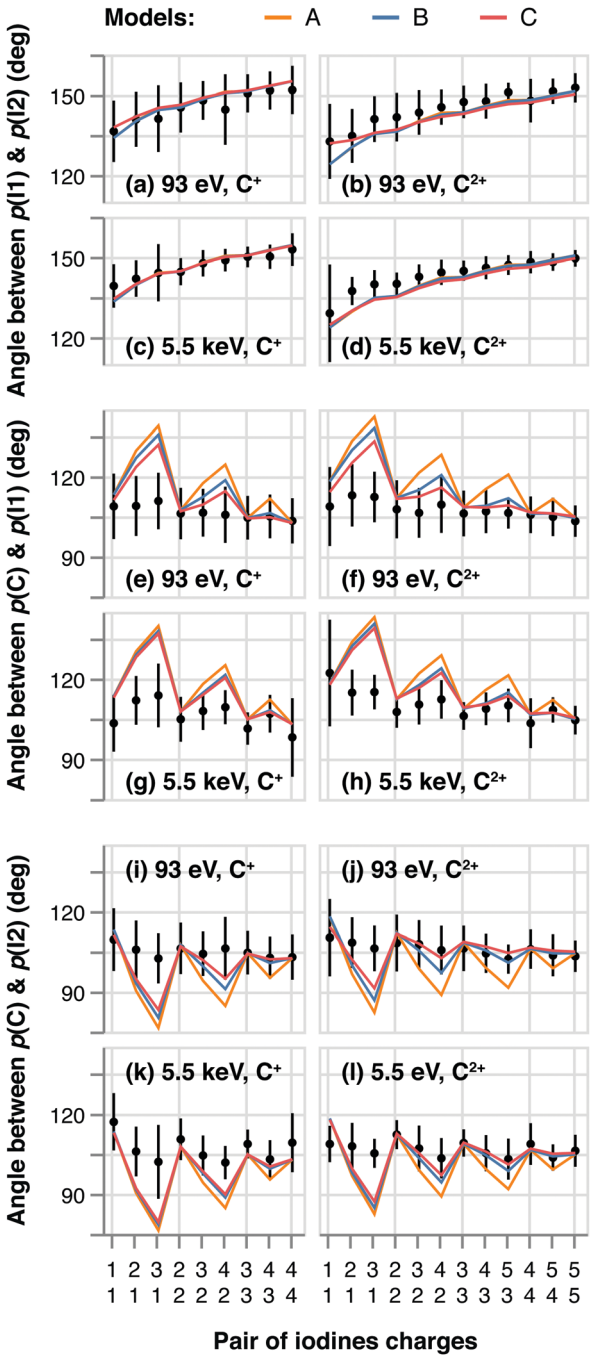

Fig. 7 Average angles between momenta of two iodine ions include (a) C^+ and (b) C^{2+} at 93 eV FEL photon energy and (c) C^+ and (d) C^{2+} at 5.5 keV, between momenta of carbon and earlier detected iodine ions include (e) C^+ and (f) C^{2+} at 93 eV FEL photon energy and (g) C^+ and (h) C^{2+} at 5.5 keV, and between momenta of carbon and later detected iodine ions include (i) C^+ and (j) C^{2+} at 93 eV FEL photon energy and (k) C^+ and (l) C^{2+} at 5.5 keV. p(C), p(I1), and p(I2) denote the momenta of carbon and earlier and later detected iodine ions, respectively. The data used to generate the experimental plots for 5.5 keV are the same as those reported in ref. 32.

Coulomb interactions between the ions are treated as point charge interaction and the concerted dynamics of charge build-up is taken into account. We assume that the total charge of the

molecule, Q_{tot}, increases as a function of time by the charge build-up time τ[31–33] according to

$$Q_{tot}(t) = Q_{max}(1 - \exp(-t/\tau)), \quad (13)$$

where Q_{max} is sum of charges of the three detected ions plus two (assuming two undetected protons). For charge distributions among the five atoms, we consider three cases as described below.

In the first model (A), the ratios of the atomic charges are kept the same as for the final charges, therefore the charge build-up constant is the same for all atoms. Best agreement of the simulations to the experimental results are found for τ = 15 fs and 10 fs for the 93 eV and 5.5 keV data, respectively, as shown in Fig. 6. Note that the obtained τ of 10 fs for the 5.5 keV data is the same as the optimal value from the comparison with the DFTB/MD simulation.[32] Model A simulations show also fairly good agreement with the experiment for the angle between the momenta of two iodine ions, while poor agreement is achieved for the angle between momenta of the carbon and iodine ions as shown in Fig. 7. However, when charges of the two iodine ions are the same, agreement is good also for the angle between momenta of the carbon and iodine ions. Discrepancies arise when difference between charges of two iodines are large. We also notice that charge-state-dependence of the experimental angles between carbon and iodine momenta are significantly smaller than the simulated dependence as shown in Fig. 7(e)–(l). It indicates that carbon ion receives similar force from the potentials created by two iodine ions.

Based on the above observations, we consider a second model (B) that treats the iodine charges differently. The carbon and hydrogen charges and sum of the two iodine charges increase with the same τ. The charges at two iodines are equal until one of them reaches its final charge – the lower one of the two iodine final charges. After that, the charge at that iodine does not change any more and only the charge of the other iodine increases with twice the initial rate constant. τ was optimised to obtain the best agreement with the average kinetic energy sum in Fig. 6 and the optimal values are 15 fs and 10 fs for the 93 eV and 5.5 keV data, respectively. Results of the model B are shown in Fig. 6 and 7. We found that the agreement with the experiment, regarding the angles between the momenta, is improved while also maintaining good agreement for the same iodine charges (Fig. 7). Regarding ion kinetic energies, the agreement of models A and B with the experiment are essentially the same (Fig. 6).

For further improvement of the modeling and physical interpretation of the results, in a third model (C) we introduce a parameter denoted as the charge redistribution rate constant R. This parameter has previously been successfully used for a molecule with a single absorption site.[31,33] In the present molecule, CH_2I_2, we assume that the charge flows from the two iodine atoms to CH_2 group that

$$\frac{dQ_{CH_2}(t)}{dt} = R \times Q_{2I}(t), \quad (14)$$

where Q_{CH_2} and Q_{2I} are sums of charges at carbon and the two hydrogen atoms and at two iodine atoms, respectively. Ratio of the charges among the carbon and the two hydrogens is kept equal the ratio of the final charges. Charges between two iodine atoms are distributed as in the model B, *i.e.*, charges at both iodine atoms are the same until one iodine reaches the final charge. Best agreement with the measured average kinetic energies were obtained with τ = 20 fs and R = 0.5 fs^{-1} for 93 eV and τ = 10 fs and R = 0.33 fs^{-1} for 5.5 keV. The results of model C are shown in Fig. 6 and 7, agreeing best with the experimental results of the three introduced models.

Although we have achieved improvement of the model, discrepancies of the angle for the low charge states are large, especially for I^+–I^{3+} and I^{2+}–I^{4+} productions. It may indicate that I^{3+} and I^{4+} are produced at large I–I distance where charges produced by photoionization at one iodine cannot move to another iodine at late part of the FEL pulse.

In all the models, τ = ~20 fs and 10 fs for the 93 eV and 5.5 keV FELs, respectively, are the optimal values. Note that the pulse duration of the 93 eV FEL pulse is ~70 fs, whereas that of the 5.5 keV FEL pulse is ~10 fs. The value of τ = 10 fs for the 5.5 keV FEL means that during the FEL pulse duration of 10 fs the molecule does not reach the final charge state. The charge of the molecule at the end of the 10 fs pulse is about 2/3 of its final charge. On the other hand, the value of τ = 20 fs for the 93 eV FEL means that during the FEL pulse duration of 70 fs the molecule reaches almost the final charge state. Those indicate that the 10 fs lies in the intermediate regime where the time scale of internal Auger decays takes part in the determination of τ, as well as the time span of sequential photoabsorption processes, while those processes terminate within 70 fs.

6 Conclusions

We have measured the momenta of fragment atomic ions released from CH_2I_2 molecules irradiated by 93 eV soft X-ray FEL pulses by multiple coincidence momentum-resolving ion TOF spectroscopy. In order to extract true correlations from the multi-hit ion data, we have formulated two-fold and three-fold covariances to use in the single-particle-counting experiments. Kinetic energy sums and angles between the ion momenta were obtained from the events producing three ions and compared with the CCE-CE simulations and also with the earlier experimental data obtained using 5.5 keV FEL pulses.[32] As a result, we obtained the time constants of 10–20 fs for the Auger decay cascades following the initial photoabsorption. In addition to the specific results presented here, we note that the covariance method, as developed here, can be used to study correlations between or involving electrons, photons from fluorescence *etc.*, not only between multiple ions. It can be applied to a wide range of target species, physical phenomena, and also to time-resolved experiments.

Author contributions

H. F. and K. U. conceived the research. D. Y., S. S., M. B., T. G., M. H., P. J., N. K., H. M., A. Ne., A. Ni., M. P., E. P., T. T., S. W.,

N. Y., K. N., and E. K. performed the experiment. S. O., K. T., and M. Y. are responsible for the SACLA and SACLA beamline. D. Y., H. F. Y. L., and S. S. analyzed the experimental data. D. Y., H. F., E. K., and K. U. prepared the manuscript with contributions from all other authors.

Conflicts of interest

There are no conflicts to declare.

Acknowledgements

The experiments were performed at the BL1 of SACLA with the approval of the Japan Synchrotron Radiation Research Institute (JASRI) and the program review committee (No. 2016B8076, 2017A8005, 2017B8065). This study was supported by the X-ray Free Electron Laser Utilization Research Project and the X-ray Free Electron Laser Priority Strategy Program of the Ministry of Education, Culture, Sports, Science and Technology of Japan (MEXT), by the Proposal Program of SACLA Experimental Instruments of RIKEN, by the Japan Society for the Promotion of Science (JSPS) KAKENHI Grant Numbers JP15K17487, JP19H04392, by ''Dynamic Alliance for Open Innovation Bridging Human, Environment and Materials'' from the MEXT, by the Research Program of ''Dynamic Alliance for Open Innovation Bridging Human, Environment and Materials'' in ''Network Joint Research Center for Materials and Devices'', and by the IMRAM project. D. Y. acknowledges support by the a Grant-in-Aid of Tohoku University Institute for Promoting Graduate Degree Programs Division for Interdisciplinary Advanced Research and Education and JSPS KAKENHI Number JP19J12870. P. J. acknowledges the financial support by the Swedish Research Council and the Swedish Foundation for Strategic Research. E. K., E. P., M. P., and M. H. acknowledge the financial support by the Academy of Finland.

References

1 W. Ackermann, G. Asova, V. Ayvazyan, A. Azima, N. Baboi, J. Bähr, V. Balandin, B. Beutner, A. Brandt, A. Bolzmann, R. Brinkmann, O. I. Brovko, M. Castellano, P. Castro, L. Catani, E. Chiadroni, S. Choroba, A. Cianchi, J. T. Costello, D. Cubaynes, J. Dardis, W. Decking, H. Delsim-Hashemi, A. Delserieys, G. Di Pirro, M. Dohlus, S. Düsterer, A. Eckhardt, H. T. Edwards, B. Faatz, J. Feldhaus, K. Flöttmann, J. Frisch, L. Fröhlich, T. Garvey, U. Gensch, C. Gerth, M. Görler, N. Golubeva, H.-J. Grabosch, M. Grecki, O. Grimm, K. Hacker, U. Hahn, J. H. Han, K. Honkavaara, T. Hott, M. Hüning, Y. Ivanisenko, E. Jaeschke, W. Jalmuzna, T. Jezynski, R. Kammering, V. Katalev, K. Kavanagh, E. T. Kennedy, S. Khodyachykh, K. Klose, V. Kocharyan, M. Körfer, M. Kollewe, W. Koprek, S. Korepanov, D. Kostin, M. Krassilnikov, G. Kube, M. Kuhlmann, C. L. S. Lewis, L. Lilje, T. Limberg, D. Lipka, F. Löhl, H. Luna, M. Luong, M. Martins, M. Meyer, P. Michelato, V. Miltchev, W. D. Möller, L. Monaco, W. F. O. Müller, O. Napieralski, O. Napoly, P. Nicolosi, D. Nölle, T. Nuñez, A. Oppelt, C. Pagani, R. Paparella, N. Pchalek, J. Pedregosa-Gutierrez, B. Petersen, B. Petrosyan, G. Petrosyan, L. Petrosyan, J. Pflüger, E. Plönjes, L. Poletto, K. Pozniak, E. Prat, D. Proch, P. Pucyk, P. Radcliffe, H. Redlin, K. Rehlich, M. Richter, M. Roehrs, J. Roensch, R. Romaniuk, M. Ross, J. Rossbach, V. Rybnikov, M. Sachwitz, E. L. Saldin, W. Sandner, H. Schlarb, B. Schmidt, M. Schmitz, P. Schmüser, J. R. Schneider, E. A. Schneidmiller, S. Schnepp, S. Schreiber, M. Seidel, D. Sertore, A. V. Shabunov, C. Simon, S. Simrock, E. Sombrowski, A. A. Sorokin, P. Spanknebel, R. Spesyvtsev, L. Staykov, B. Steffen, F. Stephan, F. Stulle, H. Thom, K. Tiedtke, M. Tischer, S. Toleikis, R. Treusch, D. Trines, I. Tsakov, E. Vogel, T. Weiland, H. Weise, M. Wellhöfer, M. Wendt, I. Will, A. Winter, K. Wittenburg, W. Wurth, P. Yeates, M. V. Yurkov, I. Zagorodnov and K. Zapfe, *Nat. Photonics*, 2007, **1**, 336–342.

2 P. Emma, R. Akre, J. Arthur, R. Bionta, C. Bostedt, J. Bozek, A. Brachmann, P. Bucksbaum, R. Coffee, F.-J. Decker, Y. Ding, D. Dowell, S. Edstrom, A. Fisher, J. Frisch, S. Gilevich, J. Hastings, G. Hays, P. Hering, Z. Huang, R. Iverson, H. Loos, M. Messerschmidt, A. Miahnahri, S. Moeller, H.-D. Nuhn, G. Pile, D. Ratner, J. Rzepiela, D. Schultz, T. Smith, P. Stefan, H. Tompkins, J. Turner, J. Welch, W. White, J. Wu, G. Yocky and J. Galayda, *Nat. Photonics*, 2010, **4**, 641–647.

3 T. Ishikawa, H. Aoyagi, T. Asaka, Y. Asano, N. Azumi, T. Bizen, H. Ego, K. Fukami, T. Fukui, Y. Furukawa, S. Goto, H. Hanaki, T. Hara, T. Hasegawa, T. Hatsui, A. Higashiya, T. Hirono, N. Hosoda, M. Ishii, T. Inagaki, Y. Inubushi, T. Itoga, Y. Joti, M. Kago, T. Kameshima, H. Kimura, Y. Kirihara, A. Kiyomichi, T. Kobayashi, C. Kondo, T. Kudo, H. Maesaka, X. M. Maréchal, T. Masuda, S. Matsubara, T. Matsumoto, T. Matsushita, S. Matsui, M. Nagasono, N. Nariyama, H. Ohashi, T. Ohata, T. Ohshima, S. Ono, Y. Otake, C. Saji, T. Sakurai, T. Sato, K. Sawada, T. Seike, K. Shirasawa, T. Sugimoto, S. Suzuki, S. Takahashi, H. Takebe, K. Takeshita, K. Tamasaku, H. Tanaka, R. Tanaka, T. Tanaka, T. Togashi, K. Togawa, A. Tokuhisa, H. Tomizawa, K. Tono, S. Wu, M. Yabashi, M. Yamaga, A. Yamashita, K. Yanagida, C. Zhang, T. Shintake, H. Kitamura and N. Kumagai, *Nat. Photonics*, 2012, **6**, 540–544.

4 E. Allaria, D. Castronovo, P. Cinquegrana, P. Craievich, M. Dal Forno, M. B. Danailov, G. D'Auria, A. Demidovich, G. De Ninno, S. Di Mitri, B. Diviacco, W. M. Fawley, M. Ferianis, E. Ferrari, L. Froehlich, G. Gaio, D. Gauthier, L. Giannessi, R. Ivanov, B. Mahieu, N. Mahne, I. Nikolov, F. Parmigiani, G. Penco, L. Raimondi, C. Scafuri, C. Serpico, P. Sigalotti, S. Spampinati, C. Spezzani, M. Svandrlik, C. Svetina, M. Trovo, M. Veronese, D. Zangrando and M. Zangrando, *Nat. Photonics*, 2013, **7**, 913–918.

5 I. S. Ko, H.-S. Kang, H. Heo, C. Kim, G. Kim, C.-K. Min, H. Yang, S. Y. Baek, H.-J. Choi, G. Mun, B. R. Park, Y. J. Suh, D. C. Shin, J. Hu, J. Hong, S. Jung, S.-H. Kim, K. Kim, D. Na, S. S. Park, Y. J. Park, Y. G. Jung, S. H. Jeong, H. G. Lee, S. Lee,

S. Lee, B. Oh, H. S. Suh, J.-H. Han, M. H. Kim, N.-S. Jung, Y.-C. Kim, M.-S. Lee, B.-H. Lee, C.-W. Sung, I.-S. Mok, J.-M. Yang, Y. W. Parc, W.-W. Lee, C.-S. Lee, H. Shin, J. H. Kim, Y. Kim, J. H. Lee, S.-Y. Park, J. Kim, J. Park, I. Eom, S. Rah, S. Kim, K. H. Nam, J. Park, J. Park, S. Kim, S. Kwon, R. An, S. H. Park, K. S. Kim, H. Hyun, S. N. Kim, S. Kim, C.-J. Yu, B.-S. Kim, T.-H. Kang, K.-W. Kim, S.-H. Kim, H.-S. Lee, H.-S. Lee, K.-H. Park, T.-Y. Koo, D.-E. Kim and K. B. Lee, *Appl. Sci.*, 2017, **7**, 479.

6 T. Tschentscher, C. Bressler, J. Grünert, A. Madsen, A. P. Mancuso, M. Meyer, A. Scherz, H. Sinn and U. Zastrau, *Appl. Sci.*, 2017, **7**, 592.

7 C. J. Milne, T. Schietinger, M. Aiba, A. Alarcon, J. Alex, A. Anghel, V. Arsov, C. Beard, P. Beaud, S. Bettoni, M. Bopp, H. Brands, M. Brönnimann, I. Brunnenkant, M. Calvi, A. Citterio, P. Craievich, M. Csatari Divall, M. Dällenbach, M. D'Amico, A. Dax, Y. Deng, A. Dietrich, R. Dinapoli, E. Divall, S. Dordevic, S. Ebner, C. Erny, H. Fitze, U. Flechsig, R. Follath, F. Frei, F. Gärtner, R. Ganter, T. Garvey, Z. Geng, I. Gorgisyan, C. Gough, A. Hauff, C. P. Hauri, N. Hiller, T. Humar, S. Hunziker, G. Ingold, R. Ischebeck, M. Janousch, P. Juranić, M. Jurcevic, M. Kaiser, B. Kalantari, R. Kalt, B. Keil, C. Kittel, G. Knopp, W. Koprek, H. T. Lemke, T. Lippuner, D. Llorente Sancho, F. Löhl, C. Lopez-Cuenca, F. Märki, F. Marcellini, G. Marinkovic, I. Martiel, R. Menzel, A. Mozzanica, K. Nass, G. L. Orlandi, C. Ozkan Loch, E. Panepucci, M. Paraliev, B. Patterson, B. Pedrini, M. Pedrozzi, P. Pollet, C. Pradervand, E. Prat, P. Radi, J.-Y. Raguin, S. Redford, J. Rehanek, J. Réhault, S. Reiche, M. Ringele, J. Rittmann, L. Rivkin, A. Romann, M. Ruat, C. Ruder, L. Sala, L. Schebacher, T. Schilcher, V. Schlott, T. Schmidt, B. Schmitt, X. Shi, M. Stadler, L. Stingelin, W. Sturzenegger, J. Szlachetko, D. Thattil, D. M. Treyer, A. Trisorio, W. Tron, S. Vetter, C. Vicario, D. Voulot, M. Wang, T. Zamofing, C. Zellweger, R. Zennaro, E. Zimoch, R. Abela, L. Patthey and H.-H. Braun, *Appl. Sci.*, 2017, **7**, 720.

8 M. M. Seibert, T. Ekeberg, F. R. N. C. Maia, M. Svenda, J. Andreasson, O. Jönsson, D. Odić, B. Iwan, A. Rocker, D. Westphal, M. Hantke, D. P. DePonte, A. Barty, J. Schulz, L. Gumprecht, N. Coppola, A. Aquila, M. Liang, T. A. White, A. Martin, C. Caleman, S. Stern, C. Abergel, V. Seltzer, J.-M. Claverie, C. Bostedt, J. D. Bozek, S. Boutet, A. A. Miahnahri, M. Messerschmidt, J. Krzywinski, G. Williams, K. O. Hodgson, M. J. Bogan, C. Y. Hampton, R. G. Sierra, D. Starodub, I. Andersson, S. Bajt, M. Barthelmess, J. C. H. Spence, P. Fromme, U. Weierstall, R. Kirian, M. Hunter, R. B. Doak, S. Marchesini, S. P. Hau-Riege, M. Frank, R. L. Shoeman, L. Lomb, S. W. Epp, R. Hartmann, D. Rolles, A. Rudenko, C. Schmidt, L. Foucar, N. Kimmel, P. Holl, B. Rudek, B. Erk, A. Hömke, C. Reich, D. Pietschner, G. Weidenspointner, L. Strüder, G. Hauser, H. Gorke, J. Ullrich, I. Schlichting, S. Herrmann, G. Schaller, F. Schopper, H. Soltau, K.-U. Kühnel, R. Andritschke, C.-D. Schröter, F. Krasniqi, M. Bott, S. Schorb, D. Rupp, M. Adolph, T. Gorkhover, H. Hirsemann, G. Potdevin, H. Graafsma, B. Nilsson, H. N. Chapman and J. Hajdu, *Nature*, 2011, **470**, 78–81.

9 N. D. Loh, C. Y. Hampton, A. V. Martin, D. Starodub, R. G. Sierra, A. Barty, A. Aquila, J. Schulz, L. Lomb, J. Steinbrener, R. L. Shoeman, S. Kassemeyer, C. Bostedt, J. Bozek, S. W. Epp, B. Erk, R. Hartmann, D. Rolles, A. Rudenko, B. Rudek, L. Foucar, N. Kimmel, G. Weidenspointner, G. Hauser, P. Holl, E. Pedersoli, M. Liang, M. S. Hunter, L. Gumprecht, N. Coppola, C. Wunderer, H. Graafsma, F. R. N. C. Maia, T. Ekeberg, M. Hantke, H. Fleckenstein, H. Hirsemann, K. Nass, T. A. White, H. J. Tobias, G. R. Farquar, W. H. Benner, S. P. Hau-Riege, C. Reich, A. Hartmann, H. Soltau, S. Marchesini, S. Bajt, M. Barthelmess, P. Bucksbaum, K. O. Hodgson, L. Strüder, J. Ullrich, M. Frank, I. Schlichting, H. N. Chapman and M. J. Bogan, *Nature*, 2012, **486**, 513–517.

10 T. Kimura, Y. Joti, A. Shibuya, C. Song, S. Kim, K. Tono, M. Yabashi, M. Tamakoshi, T. Moriya, T. Oshima, T. Ishikawa, Y. Bessho and Y. Nishino, *Nat. Commun.*, 2014, **5**, 3052.

11 R. Mankowsky, A. Subedi, M. Först, S. O. Mariager, M. Chollet, H. T. Lemke, J. S. Robinson, J. M. Glownia, M. P. Minitti, A. Frano, M. Fechner, N. A. Spaldin, T. Loew, B. Keimer, A. Georges and A. Cavalleri, *Nature*, 2014, **516**, 71–73.

12 K. H. Kim, J. G. Kim, S. Nozawa, T. Sato, K. Y. Oang, T. W. Kim, H. Ki, J. Jo, S. Park, C. Song, T. Sato, K. Ogawa, T. Togashi, K. Tono, M. Yabashi, T. Ishikawa, J. Kim, R. Ryoo, J. Kim, H. Ihee and S.-i. Adachi, *Nature*, 2015, **518**, 385–389.

13 P. Wernet, K. Kunnus, I. Josefsson, I. Rajkovic, W. Quevedo, M. Beye, S. Schreck, S. Grübel, M. Scholz, D. Nordlund, W. Zhang, R. W. Hartsock, W. F. Schlotter, J. J. Turner, B. Kennedy, F. Hennies, F. M. F. de Groot, K. J. Gaffney, S. Techert, M. Odelius and A. Föhlisch, *Nature*, 2015, **520**, 78–81.

14 T. R. M. Barends, L. Foucar, A. Ardevol, K. Nass, A. Aquila, S. Botha, R. B. Doak, K. Falahati, E. Hartmann, M. Hilpert, M. Heinz, M. C. Hoffmann, J. Köfinger, J. E. Koglin, G. Kovacsova, M. Liang, D. Milathianaki, H. T. Lemke, J. Reinstein, C. M. Roome, R. L. Shoeman, G. J. Williams, I. Burghardt, G. Hummer, S. Boutet and I. Schlichting, *Science*, 2015, **350**, 445–450.

15 E. Matsubara, S. Okada, T. Ichitsubo, T. Kawaguchi, A. Hirata, P. F. Guan, K. Tokuda, K. Tanimura, T. Matsunaga, M. W. Chen and N. Yamada, *Phys. Rev. Lett.*, 2016, **117**, 135501.

16 R. Neutze, R. Wouts, D. van der Spoel, E. Weckert and J. Hajdu, *Nature*, 2000, **406**, 752–757.

17 H. M. Quiney and K. A. Nugent, *Nat. Phys.*, 2011, **7**, 142–146.

18 B. Ziaja, H. N. Chapman, R. Fäustlin, S. Hau-Riege, Z. Jurek, A. V. Martin, S. Toleikis, F. Wang, E. Weckert and R. Santra, *New J. Phys.*, 2012, **14**, 115015.

19 L. Young, E. P. Kanter, B. Krässig, Y. Li, A. M. March, S. T. Pratt, R. Santra, S. H. Southworth, N. Rohringer, L. F. DiMauro, G. Doumy, C. A. Roedig, N. Berrah, L. Fang,

M. Hoener, P. H. Bucksbaum, J. P. Cryan, S. Ghimire, J. M. Glownia, D. A. Reis, J. D. Bozek, C. Bostedt and M. Messerschmidt, *Nature*, 2010, **466**, 56–61.

20 M. Hoener, L. Fang, O. Kornilov, O. Gessner, S. T. Pratt, M. Gühr, E. P. Kanter, C. Blaga, C. Bostedt, J. D. Bozek, P. H. Bucksbaum, C. Buth, M. Chen, R. Coffee, J. Cryan, L. DiMauro, M. Glownia, E. Hosler, E. Kukk, S. R. Leone, B. McFarland, M. Messerschmidt, B. Murphy, V. Petrovic, D. Rolles and N. Berrah, *Phys. Rev. Lett.*, 2010, **104**, 253002.

21 B. Rudek, S.-K. Son, L. Foucar, S. W. Epp, B. Erk, R. Hartmann, M. Adolph, R. Andritschke, A. Aquila, N. Berrah, C. Bostedt, J. Bozek, N. Coppola, F. Filsinger, H. Gorke, T. Gorkhover, H. Graafsma, L. Gumprecht, A. Hartmann, G. Hauser, S. Herrmann, H. Hirsemann, P. Holl, A. Hömke, L. Journel, C. Kaiser, N. Kimmel, F. Krasniqi, K.-U. Kühnel, M. Matysek, M. Messerschmidt, D. Miesner, T. Möller, R. Moshammer, K. Nagaya, B. Nilsson, G. Potdevin, D. Pietschner, C. Reich, D. Rupp, G. Schaller, I. Schlichting, C. Schmidt, F. Schopper, S. Schorb, C.-D. Schröter, J. Schulz, M. Simon, H. Soltau, L. Strüder, K. Ueda, G. Weidenspointner, R. Santra, J. Ullrich, A. Rudenko and D. Rolles, *Nat. Photonics*, 2012, **6**, 858–865.

22 H. Thomas, A. Helal, K. Hoffmann, N. Kandadai, J. Keto, J. Andreasson, B. Iwan, M. Seibert, N. Timneanu, J. Hajdu, M. Adolph, T. Gorkhover, D. Rupp, S. Schorb, T. Möller, G. Doumy, L. F. DiMauro, M. Hoener, B. Murphy, N. Berrah, M. Messerschmidt, J. Bozek, C. Bostedt and T. Ditmire, *Phys. Rev. Lett.*, 2012, **108**, 133401.

23 T. Gorkhover, M. Adolph, D. Rupp, S. Schorb, S. W. Epp, B. Erk, L. Foucar, R. Hartmann, N. Kimmel, K.-U. Kühnel, D. Rolles, B. Rudek, A. Rudenko, R. Andritschke, A. Aquila, J. D. Bozek, N. Coppola, T. Erke, F. Filsinger, H. Gorke, H. Graafsma, L. Gumprecht, G. Hauser, S. Herrmann, H. Hirsemann, A. Hömke, P. Holl, C. Kaiser, F. Krasniqi, J.-H. Meyer, M. Matysek, M. Messerschmidt, D. Miessner, B. Nilsson, D. Pietschner, G. Potdevin, C. Reich, G. Schaller, C. Schmidt, F. Schopper, C. D. Schröter, J. Schulz, H. Soltau, G. Weidenspointner, I. Schlichting, L. Strüder, J. Ullrich, T. Möller and C. Bostedt, *Phys. Rev. Lett.*, 2012, **108**, 245005.

24 B. Erk, D. Rolles, L. Foucar, B. Rudek, S. W. Epp, M. Cryle, C. Bostedt, S. Schorb, J. Bozek, A. Rouzee, A. Hundertmark, T. Marchenko, M. Simon, F. Filsinger, L. Christensen, S. De, S. Trippel, J. Küpper, H. Stapelfeldt, S. Wada, K. Ueda, M. Swiggers, M. Messerschmidt, C. D. Schröter, R. Moshammer, I. Schlichting, J. Ullrich and A. Rudenko, *Phys. Rev. Lett.*, 2013, **110**, 053003.

25 H. Fukuzawa, S.-K. Son, K. Motomura, S. Mondal, K. Nagaya, S. Wada, X.-J. Liu, R. Feifel, T. Tachibana, Y. Ito, M. Kimura, T. Sakai, K. Matsunami, H. Hayashita, J. Kajikawa, P. Johnsson, M. Siano, E. Kukk, B. Rudek, B. Erk, L. Foucar, E. Robert, C. Miron, K. Tono, Y. Inubushi, T. Hatsui, M. Yabashi, M. Yao, R. Santra and K. Ueda, *Phys. Rev. Lett.*, 2013, **110**, 173005.

26 K. Tamasaku, E. Shigemasa, Y. Inubushi, T. Katayama, K. Sawada, H. Yumoto, H. Ohashi, H. Mimura, M. Yabashi, K. Yamauchi and T. Ishikawa, *Nat. Photonics*, 2014, **8**, 313–316.

27 T. Tachibana, Z. Jurek, H. Fukuzawa, K. Motomura, K. Nagaya, S. Wada, P. Johnsson, M. Siano, S. Mondal, Y. Ito, M. Kimura, T. Sakai, K. Matsunami, H. Hayashita, J. Kajikawa, X.-J. Liu, E. Robert, C. Miron, R. Feifel, J. P. Marangos, K. Tono, Y. Inubushi, M. Yabashi, S.-K. Son, B. Ziaja, M. Yao, R. Santra and K. Ueda, *Sci. Rep.*, 2015, **5**, 10977.

28 H. Yoneda, Y. Inubushi, K. Nagamine, Y. Michine, H. Ohashi, H. Yumoto, K. Yamauchi, H. Mimura, H. Kitamura, T. Katayama, T. Ishikawa and M. Yabashi, *Nature*, 2015, **524**, 446–449.

29 A. Rudenko, L. Inhester, K. Hanasaki, X. Li, S. J. Robatjazi, B. Erk, R. Boll, K. Toyota, Y. Hao, O. Vendrell, C. Bomme, E. Savelyev, B. Rudek, L. Foucar, S. H. Southworth, C. S. Lehmann, B. Kraessig, T. Marchenko, M. Simon, K. Ueda, K. R. Ferguson, M. Bucher, T. Gorkhover, S. Carron, R. Alonso-Mori, J. E. Koglin, J. Correa, G. J. Williams, S. Boutet, L. Young, C. Bostedt, S.-K. Son, R. Santra and D. Rolles, *Nature*, 2017, **546**, 129–132.

30 B. Rudek, K. Toyota, L. Foucar, B. Erk, R. Boll, C. Bomme, J. Correa, S. Carron, S. Boutet, G. J. Williams, K. R. Ferguson, R. Alonso-Mori, J. E. Koglin, T. Gorkhover, M. Bucher, C. S. Lehmann, B. Kråssig, S. H. Southworth, L. Young, C. Bostedt, K. Ueda, T. Marchenko, M. Simon, Z. Jurek, R. Santra, A. Rudenko, S.-K. Son and D. Rolles, *Nat. Commun.*, 2018, **9**, 4200.

31 K. Motomura, E. Kukk, H. Fukuzawa, S. Wada, K. Nagaya, S. Ohmura, S. Mondal, T. Tachibana, Y. Ito, R. Koga, T. Sakai, K. Matsunami, A. Rudenko, C. Nicolas, X.-J. Liu, C. Miron, Y. Zhang, Y. H. Jiang, J. Chen, M. Anand, D.-E. Kim, K. Tono, M. Yabashi, M. Yao and K. Ueda, *J. Phys. Chem. Lett.*, 2015, **6**, 2944–2949.

32 T. Takanashi, K. Nakamura, E. Kukk, K. Motomura, H. Fukuzawa, K. Nagaya, S.-i. Wada, Y. Kumagai, D. Iablonskyi, Y. Ito, Y. Sakakibara, D. You, T. Nishiyama, K. Asa, Y. Sato, T. Umemoto, K. Kariyazono, K. Ochiai, M. Kanno, K. Yamazaki, K. Kooser, C. Nicolas, C. Miron, T. Asavei, L. Neagu, M. Schöffler, G. Kastirke, X.-J. Liu, A. Rudenko, S. Owada, T. Katayama, T. Togashi, K. Tono, M. Yabashi, H. Kono and K. Ueda, *Phys. Chem. Chem. Phys.*, 2017, **19**, 19707–19721.

33 K. Nagaya, K. Motomura, E. Kukk, H. Fukuzawa, S. Wada, T. Tachibana, Y. Ito, S. Mondal, T. Sakai, K. Matsunami, R. Koga, S. Ohmura, Y. Takahashi, M. Kanno, A. Rudenko, C. Nicolas, X.-J. Liu, Y. Zhang, J. Chen, M. Anand, Y. H. Jiang, D.-E. Kim, K. Tono, M. Yabashi, H. Kono, C. Miron, M. Yao and K. Ueda, *Phys. Rev. X*, 2016, **6**, 021035.

34 K. Nagaya, K. Motomura, E. Kukk, Y. Takahashi, K. Yamazaki, S. Ohmura, H. Fukuzawa, S. Wada, S. Mondal, T. Tachibana, Y. Ito, R. Koga, T. Sakai, K. Matsunami, K. Nakamura, M. Kanno, A. Rudenko, C. Nicolas, X.-J. Liu, C. Miron, Y. Zhang, Y. Jiang, J. Chen, M. Anand, D. E. Kim, K. Tono, M. Yabashi, M. Yao, H. Kono and K. Ueda, *Faraday Discuss.*, 2016, **194**, 537–562.

35 E. Kukk, H. Myllynen, K. Nagaya, S. Wada, J. D. Bozek, T. Takanashi, D. You, A. Niozu, K. Kooser, T. Gaumnitz,

E. Pelimanni, M. Berholts, S. Granroth, N. Yokono, H. Fukuzawa, C. Miron and K. Ueda, *Phys. Rev. A*, 2019, **99**, 023411.

36 L. J. Frasinski, K. Codling and P. A. Hatherly, *Science*, 1989, **246**, 1029–1031.

37 G. Prümper and K. Ueda, *Nucl. Instrum. Methods Phys. Res., Sect. A*, 2007, **574**, 350–362.

38 V. Zhaunerchyk, L. J. Frasinski, J. H. D. Eland and R. Feifel, *Phys. Rev. A: At., Mol., Opt. Phys.*, 2014, **89**, 053418.

39 E. Kukk, K. Motomura, H. Fukuzawa, K. Nagaya and K. Ueda, *Appl. Sci.*, 2017, **7**, 531.

40 S. Owada, K. Togawa, T. Inagaki, T. Hara, T. Tanaka, Y. Joti, T. Koyama, K. Nakajima, H. Ohashi, Y. Senba, T. Togashi, K. Tono, M. Yamaga, H. Yumoto, M. Yabashi, H. Tanaka and T. Ishikawa, *J. Synchrotron Radiat.*, 2018, **25**, 282–288.

41 H. Fukuzawa, K. Nagaya and K. Ueda, *Nucl. Instrum. Methods Phys. Res., Sect. A*, 2018, **907**, 116–131.

42 O. Jagutzki, A. Cerezo, A. Czasch, R. Dörner, M. Hattaß, M. Huang, V. Mergel, U. Spillmann, K. Ullmann-Pfleger, T. Weber, H. Schmidt-Böcking and G. D. W. Smith, *IEEE Trans. Nucl. Sci.*, 2002, **49**, 2477–2483.

43 A. T. J. B. Eppink and D. H. Parker, *Rev. Sci. Instrum.*, 1997, **68**, 3477–3484.

44 K. Motomura, L. Foucar, A. Czasch, N. Saito, O. Jagutzki, H. Schmidt-Böcking, R. Dörner, X.-J. Liu, H. Fukuzawa, G. Prümper, K. Ueda, M. Okunishi, K. Shimada, T. Harada, M. Toyoda, M. Yanagihara, M. Yamamoto, H. Iwayama, K. Nagaya, M. Yao, A. Rudenko, J. Ullrich, M. Nagasono, A. Higashiya, M. Yabashi, T. Ishikawa, H. Ohashi and H. Kimura, *Nucl. Instrum. Methods Phys. Res., Sect. A*, 2009, **606**, 770–773.

